Structural And Magnetic Properties Of Some Vacancy Ordered Osmium Halide Perovskites

Matilde Saura-Múzquiz[1,2], Maxim Avdeev[1,3], Helen E. A. Brand[4] and Brendan J. Kennedy[1*]

[1] School of Chemistry, The University of Sydney, Sydney, New South Wales 2006, Australia

[2] Department of Materials Physics, Universidad Complutense de Madrid, 28040, Madrid, Spain

[3] Australian Nuclear Science and Technology Organisation, New Illawarra Rd., Lucas Heights, New South Wales 2234, Australia

[4] Australian Synchrotron, Australian Nuclear Science and Technology Organisation, 800 Blackburn Road, Clayton, Victoria 3168, Australia

[*] Corresponding Author: Brendan J. Kennedy (brendan.kennedy@sydney.edu.au)

Abstract

The structures and magnetic properties of the Os^{4+} ($5d^4$) halides K_2OsCl_6, K_2OsBr_6, Na_2OsBr_6 and $Na_2OsBr_6.6H_2O$ are described. K_2OsCl_6 and K_2OsBr_6 have a cubic vacancy-ordered double perovskites structure but undergo different symmetry lowering structural phase transitions upon cooling associated with a combination of the relative size of the ions and differences in their chemical bonding. The structure of $Na_2OsBr_6.6H_2O$ has been determined for the first time and the thermal stability of this established using a combination of *in-situ* diffraction and TGA. $Na_2OsBr_6.6H_2O$ and Na_2OsBr_6 are isostructural with the analogous iridium chlorides, $Na_2IrCl_6.6H_2O$ and Na_2IrCl_6, dehydration proceeds *via* different intermediate phases. The magnetic moments of four compounds display Kotani-like behaviour consistent with a $J_{eff} = 0$ ground state, however the magnetic susceptibility measurements reveal unusual low temperature properties indicative of a weakly magnetic ground state.

Introduction

The solid-state chemistry of systems containing 4*d* or 5*d* transition metals is currently of considerable interest.[1] In going from the more commonly studied 3*d* elements to the 5*d* elements, the *d* orbitals become spatially more extended. This results in strong hybridisation between the 5*d* orbitals and neighbouring ligand atoms, leading to a large crystal field splitting, Δ. In an octahedral crystal field, the five *d* states are split into a triplet t_{2g} and doublet e_g level. In the 5*d* elements the crystal field splitting is much larger than the Spin Pairing Energy (Hund's coupling J_H) so that, for $d^1 - d^6$ configurations, the e_g orbitals are unoccupied. Spin-orbit coupling (SOC), that couples the total spin S determined by Hund's rule, with the (effective) orbital moment L is significant in the 4*d* or 5*d* elements and can give rise to exotic and unanticipated properties.[1-5] In the case of isolated Os(IV), d^4, ions the large crystal field and Hund's rules predict the 5*d* electrons will occupy the t_{2g} levels with threefold orbital degeneracy, $^3T_{1g}$, described by an effective orbital moment L = 1 and S = 1. If the SOC is sufficiently large this nine-fold degenerate state is split into a singlet, J = 0, ground state, with triplet and quintet excited states illustrated in scheme 1.[6] An alternate description is that the Os(IV) ions have fully occupied J_{eff} = 3/2 ground state giving J = 0 with the excited J = ½ state unoccupied See Figure S1.

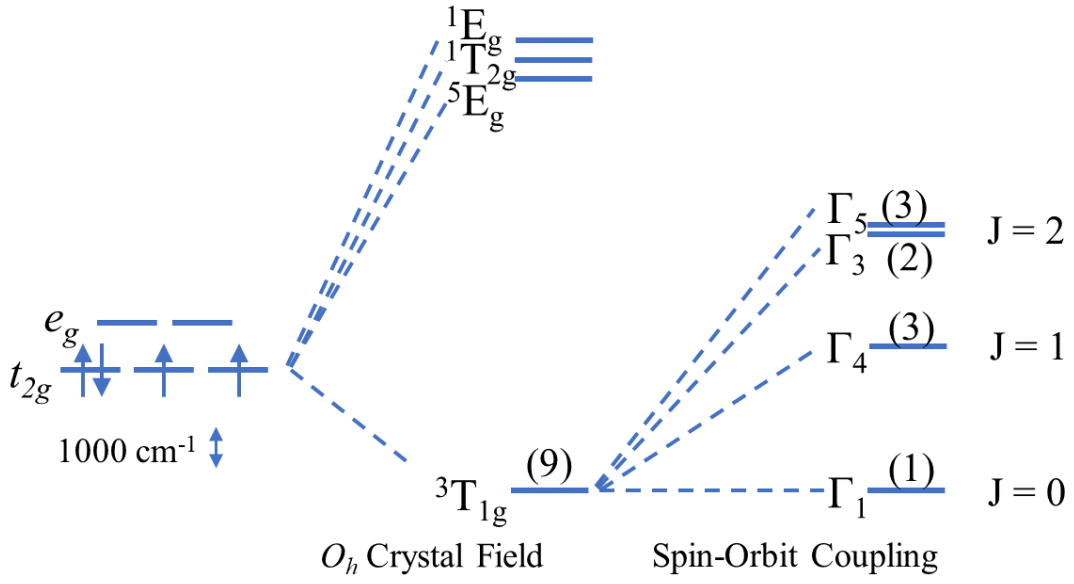

Scheme 1. Approximate energy splitting diagram for the $5d^4$ configuration of the Os^{4+} cation. The strong ligand field results in a $(t_{2g})^4(e_g)^0$ configuration, corresponding to a $^3T_{1g}$ ground state

with an excited ^5E_g state. Spin orbit coupling results in a Γ_1 level with J = 0 The numbers in parentheses are the numbers of degenerate multielectron states.

K_2OsCl_6 belongs to the K_2PtCl_6 family of antifluorite type A_2MX_6 hexahalides that features isolated MX_6 octahedra separated by alkali metal cations. An alternate description of the structure is as a rock salt ordered double perovskite of the type $A_2BB'X_6$ where the *B*' site is vacant, leading to the nomenclature of vacancy-ordered double perovskites.[7] Irrespective of the description the MX_6 octahedra are arranged on a face centre cubic lattice. The structure, magnetic and electronic properties of these types of halides, especially those containing Ir(IV) (d^5) cations, are fascinating as they combine the geometrically frustrated arrangement of the Ir(IV) cation that has a $J_{eff} = 1/2$ ground state with sizable exchange anisotropy. K_2IrCl_6 retains cubic symmetry down to very low temperatures (0.3 K) whereas K_2IrBr_6 is cubic ($Fm\bar{3}m$) at room temperature but monoclinic ($P2_1/n$) at low temperatures.[8] However, both these halides undergo antiferromagnetic ordering at low temperatures, 3.1 and 11.4 K respectively,[3] and the importance of the lower symmetry on the magnetic and electronic properties is unclear.

Bao *et al*.[9] recently described a comprehensive investigation of Na_2IrCl_6, which is readily hydrated to form two stable phases; $Na_2IrCl_6.2\ H_2O$ and $Na_2IrCl_6.6\ H_2O$. The magnetic properties of these were found to be sensitive to the degree of hydration with the hexahydrate being paramagnetic down to 1.8 K whereas the other halides studied were canted antiferromagnets. At room temperature the smaller size of the sodium cations induces cooperative tilting of the $IrCl_6$ octahedra in Na_2IrCl_6 which has the same monoclinic structure observed for K_2IrBr_6 at low temperatures.[9] The magnetic ordering temperature of Na_2IrCl_6 is reported to be 7.4 K.[9]

Johannesen and Candela[10] noted the temperature independence of the magnetic susceptibility of K_2OsCl_6 as early as 1963 and concluded that its magnetic properties were broadly in accord with Kotani theory.[11] Subsequently it was shown that K_2OsCl_6 undergoes a symmetry lowering phase transition to a tetragonal structure described in $I4/m$ on cooling to ~ 46 K. This transition was described as being a consequence of cooperative rotation of the $OsCl_6$ octahedra about the *c*-axis.[12] Recently Seshadri, Cheetham and co-workers [13-14] extended the early studies of Figgis *et al*.[15] on ruthenium halides to include some hybrid ruthenium halide perovskites and they showed that these displayed largely temperature independent magnetic moments that were consistent with the Kotani model for isolated low

spin d^5 Ru(III) ions. Unlike the iridium halides, that have a $J_{eff} = ½$ ground state, the ruthenium halides did not show evidence for magnetic ordering at low temperatures.[16]

Interest in the hexahalides has been further driven by the discovery of the remarkable optoelectronic properties of halide perovskites with formula ABX_3 (A = Cs^+, $NH_3CH_3^+$; B = Pb^{2+}; X = Cl^-, Br^-, I^-) and these have been heavily investigated due to their exceptional potential for solar energy conversion.[17] The optoelectronic properties of some lead free double perovskites, including vacancy-ordered systems, containing more benign metal cations such as Ag, Sb, and Bi are likewise of immense interest.[18-20]

Compared to the heavier 5*d* elements with a d^5 configuration (Ir^{IV} or Os^V), information on the analogous Os^{IV} (d^4) compounds is sparse. [21] In the present work we have investigated the structure and magnetic properties of some osmium compounds of the type K_2OsX_6 (X = Cl or Br) and of hydrated and dehydrated $Na_2OsBr_6.nH_2O$.

Experimental:

Samples of K_2OsCl_6, K_2OsBr_6 and $Na_2OsBr_6.6H_2O$ were purchased from Surepure Chemicals and used as received. Synchrotron X-ray diffraction (S-XRD) data were measured on the Powder Diffractometer BL-10 at the Australian Synchrotron using 21.0 keV photons, corresponding to 0.590442 Å based on Rietveld Refinement of LaB_6 NIST SRM660B line profile standard.[22] This refinement, using the Thompson-Cox-Hastings profile function,[23] also supplied the instrument resolution function. The diffractometer uses an array of 16 Mythen II microstrip detector modules. To eliminate the gap between individual modules two data sets were collected with the detector assembly shifted by 0.5°. The resulting data sets were merged using bespoke software.[22] Each sample was placed in a 0.2 mm capillary that was rotated during the measurement to minimize preferred orientation effects. Temperature control was achieved using an Oxford Cryosystems cryostream 700.

Neutron Powder Diffraction (NPD) patterns were measured using neutrons of wavelength 1.6215 Å on the high resolution diffractometer, Echidna, at ANSTO's OPAL reactor.[24]

Rietveld refinements were undertaken using the program GSAS with the EXPGUI interface.[25-26] The background was modelled by a twelfth order (S-XRD) or sixth order (NPD) shifted Chebyshev polynomial. In the final refinement cycles, the profile and lattice parameter were released and no constraints were placed on the atomic coordinates.

The magnetic properties of the powder samples were measured using a DynaCool Quantum Design Physical Property Measurement (PPMS) system equipped with a vibrating sample magnetometer (VSM). The powders were packed into a polycarbonate capsule (VSM Powder Sample Holder P125E) snapped into a brass half-tube sample holder. Zero-field-cooled (ZFC)/field-cooled (FC) curves were collected in the temperature range of 2.0 K – 300 K using an applied magnetic field of 1.0 T. Isothermal magnetization data were collected at 2.5 K, scanning the applied field in the range of $\pm$9 T.

Symmetry-adapted distortion mode analysis was performed using AMPLIMODES.[27]

Results and Discussion

1. Structural Properties

The S-XRD profile of K_2OsCl_6 measured between 90 and 300 K showed the material to retain cubic symmetry over this temperature range. In the cubic $Fm\bar{3}m$ model, illustrated in Figure 1, the Os cation is surrounded by 6 equidistant Cl anions. Anisotropic atomic displacement parameters (ADP) for the chloride anion were employed in the structural refinement and these revealed greater displacement perpendicular to the Os-Cl direction than parallel to this. *i.e.* $U^{11} < U^{22}$, further details are given in Table S1. Similar anisotropy in the ADP was described by Khan *et al.*[8, 28] for K_2IrCl_6 and this reflects the local environment of the anions, analogous to that the described in detail for rutile type oxides.[29] Intriguingly the Os-Cl distance decreases slightly on heating, from 2.3259(7) Å at 90 K to 2.3207(7) Å at 300 K, see Figure 2. The apparent contraction in this distance reflects the increased thermal vibration of the $OsCl_6$ octahedra and is ascribed to thermally activated rotational disorder. Rotational disorder of rigid polyhedra has been shown to result in apparent bond lengths contraction,[30-32] or in extreme cases, as illustrated for the *A*-site vacant perovskite ScF_3, this can lead to negative thermal expansion over a wide temperature range.[33]

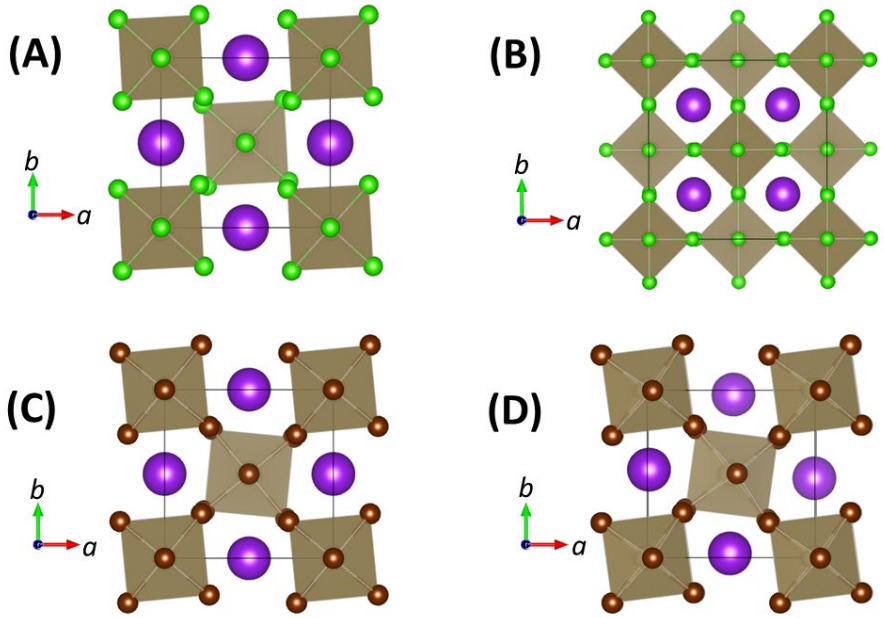

Figure 1. Representation of the structure of (A) the *I*4/*m* structure of K_2OsCl_6 at 3K, (B) the $Fm\bar{3}m$ of K_2OsCl_6 at 300 K, (C) the *P*4/*mnc* structure of K_2OsBr_6 at 187 K and (D) the $P2_1/n$ structure of K_2OsBr_6 at 90 K. In all cases the Os cations are at the centre of the polyhedral and the purple spheres represent the K atoms. The smaller brown and green spheres represent the Br and Cl anions respectively.

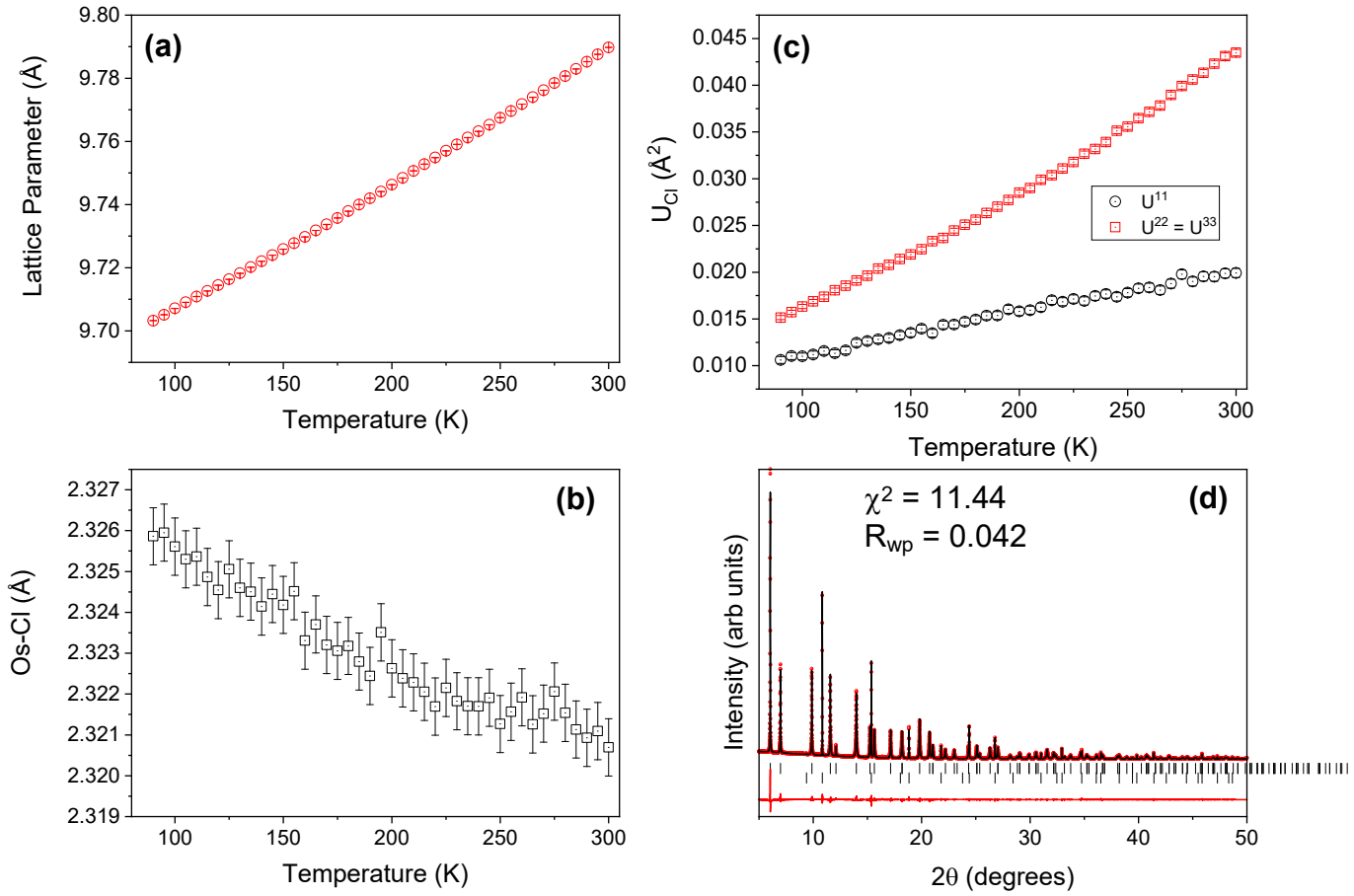

Figure 2. Temperature dependence of (a) the unit cell parameter, (b) Os-Cl distance and (c) the anisotropic atomic displacement parameters of the chloride anion in K_2OsCl_6. That U^{11} is smaller than U^{22} indicates that displacement ellipsoid perpendicular to the Os-Cl bond is greater than that parallel to the bond and this increased rotation is responsible for the reduction in the Os-Cl distance upon heating. (d) Shows an example of the Rietveld refinement in which the lower set of tick marks show peaks due to the presence of KCl in the sample. Where not apparent the esds are smaller than the symbols.

At room temperature K_2OsBr_6 adopts the same cubic structure displayed by K_2OsCl_6, albeit with a larger unit cell parameter of 10.32961(2) Å, compared with 9.78977 (3) Å in K_2OsCl_6, reflecting the larger size of the bromide anion. These values are in fair agreement

with the early report by Turner and co-workers.[34] This cubic structure is retained on cooling to about 220 K and over this temperature range U^{11} is less than U^{22} as seen for K_2OsCl_6, but in this case the Os-Br distance is essentially independent of temperature, changing from 2.4620(6) Å at 300 K to 2.4605(6) Å at 220 K. Upon cooling below 200 K additional reflections emerged most obviously near 2θ = 10.4 and 12.3º, see Figure 3, indicative of a lowering in symmetry. These were accompanied by the broadening of selected reflections, as illustrated for the $(400)_p$ reflection, as indexed on the $Fm\bar{3}m$ parent, near 13º in Figure 3. With further cooling this rapidly became a resolved doublet. That the cubic $(222)_p$ reflection near 11.4 º remained a single peak suggest the structure was tetragonal and the relative intensities of the peaks shows this to have $c/a > 1$. A model in $P4/mnc$ provided a satisfactory fit. It should be noted that the alternate ($I4/m$) tetragonal model proposed for the low temperature structure of K_2OsCl_6,[12] does not allow for the observed weak reflections near 2θ = 10.4 and 12.3º, that were indexed as the $(210)_t$ and $(212)_t$ reflections respectively. These two tetragonal models differ in their sense of the rotation of the octahedra. In $I4/m$ the rotations of the $OsCl_6$ octahedra about the c-axis are out-of-phase ($a^0a^0c^-$ in Glazer's [35] notation) whereas in $P4/mnc$ they are in-phase ($a^0a^0c^+$). We return to the tetragonal $I4/m$ structure below. Around 200 K further splitting of the $(222)_p$ reflection is observed and at 90 K this appears as a triplet, Figure 3. The $(222)_p$ reflection remains a doublet at this temperature indicating the structure to be monoclinic and a model in $P2_1/n$ proved satisfactory.[36] The observed sequence of phase transitions is the same as that reported for K_2IrBr_6.[3, 8] This monoclinic structure contains a combination of in-phase and out-of-phase tilts of the $OsBr_6$ octahedra ($a^-a^-c^+$) that can be quantified, by the corresponding symmetry-adapted distortion modes formalism. Seven irreducible representations can contribute to the symmetry breaking from the high symmetry cubic phase to the monoclinic phase: GM_1^+, GM_3^+, GM_4^+, GM_5^+, X_2^+, $X_3^+$and X_5^+. The GM_4^+ single mode describes rotation of the octahedra around the b axis and is associated with out of phase tilting of the $OsBr_6$ octahedra, see Table S2. The X_3^+mode describes rotation around the c-axis and is associated with the in-phase tilting of the octahedra. In K_2OsBr_6 the magnitude of GM_4^+ is smaller than that of the X_3^+ single mode suggesting that the out-of-phase tilts will be lost before the in-phase tilts as the sample transforms from monoclinic to cubic upon heating. This is consistent with the observation of the $P4/mnc$ phase around 210 K that only contains in-phase tilts that are described by the primary mode X_3^+.

Establishing the precise temperature of the phase transitions from the diffraction data proved challenging as both the $Fm\bar{3}m$ ($a^0a^0a^0$) to *P*4/*mnc* ($a^0a^0c^+$) and *P*4/*mnc* ($a^0a^0c^+$) to $P2_1/n$ ($a^-a^-c^+$) transitions are allowed to be continuous.[37] The temperature dependence of the monoclinic angle, illustrated in Figure 3, was well produced by an expression of the type $90 - \beta = A(T_c - T)^\eta$ with $\eta = 0.5$ indicative of a continuous second order phase transition. Based on this fit we estimate the $P2_1/n$ to *P*4/*mnc* transition occurs at 197(1) K. Around 220 K, that is near the tetragonal to cubic phase transition there was a small, but discernable, increase in the Rietveld R-factors obtained when using the tetragonal *P*4/*mnc* model, see Figure S2. Scrutiny of the profiles did not reveal the emergence, or loss, of any reflections in this temperature range, although the reflections diagnostic of the out-of-phase tilts such as the (210) and (212) reflections rapidly lost intensity. By symmetry, there is an intermediate *I*4/*mmm* structure between *P*4/*mnc* and $Fm\bar{3}m$, however this is unlikely to be present, since the amplitude of the corresponding GM_3^+ is much smaller than that of X_3^+, corresponding to *P*4/*mnc*, which goes to zero at the tetragonal to cubic transition. The observed changes are not indicative of the presence of an intermediate phase. Rather it appears that the transition to the cubic structure involves a small (~ 10 K) two-phase region and satisfactory fits could be obtained to a two phase *P*4/*mnc* and $Fm\bar{3}m$ model, see Figure S3. Numerous structural studies of perovskites have demonstrated that when a transition that involves condensation of a soft mode is symmetry allowed to be continuous, it invariably is. Although the general topology of the K_2PtCl_6 type structures is the same as that of the $A_2BB'X_6$ rock-salt ordered double perovskites, there is an absence of corner sharing connectivity of the BX_6 network in the K_2PtCl_6 type structures. This appears to impact the coherence of the cooperative tilting of these leading to the co-existence of the cubic and tetragonal phases over a limited temperature range. This observation is somewhat similar to the observation of phase co-existence in some ABO_4 scheelite type oxides that contain isolated BO_4 tetrahedra between the low symmetry *I*2/*a* and higher symmetry *I*4/*a* phases near their structural phase transition.[38] Since the cell metric of the tetragonal and cubic phases of K_2OsBr_6 phases are essentially identical in the temperature range of interest, quantification of the two phases was not possible.

Once the phase behaviour of K_2OsBr_6 was established, Rietveld refinements for all data were undertaken and the temperature dependence of the lattice parameters from such refinements is illustrated in Figure 3. Figure 4 illustrates the temperature dependence of the

average Os-Br distance. Both figures are remarkable for the dramatic changes across the tetragonal phase. Figure 4 shows that, upon cooling, the Os-Br distance in the cubic phase is only weakly dependent on temperature. However, in the tetragonal phase (between ~ 197 and 220 K) it rapidly increases upon cooling. Once the transition to the monoclinic structure occurs the average Os-Br distance shows expected behaviour of slowly contracting as the temperature is lowered.

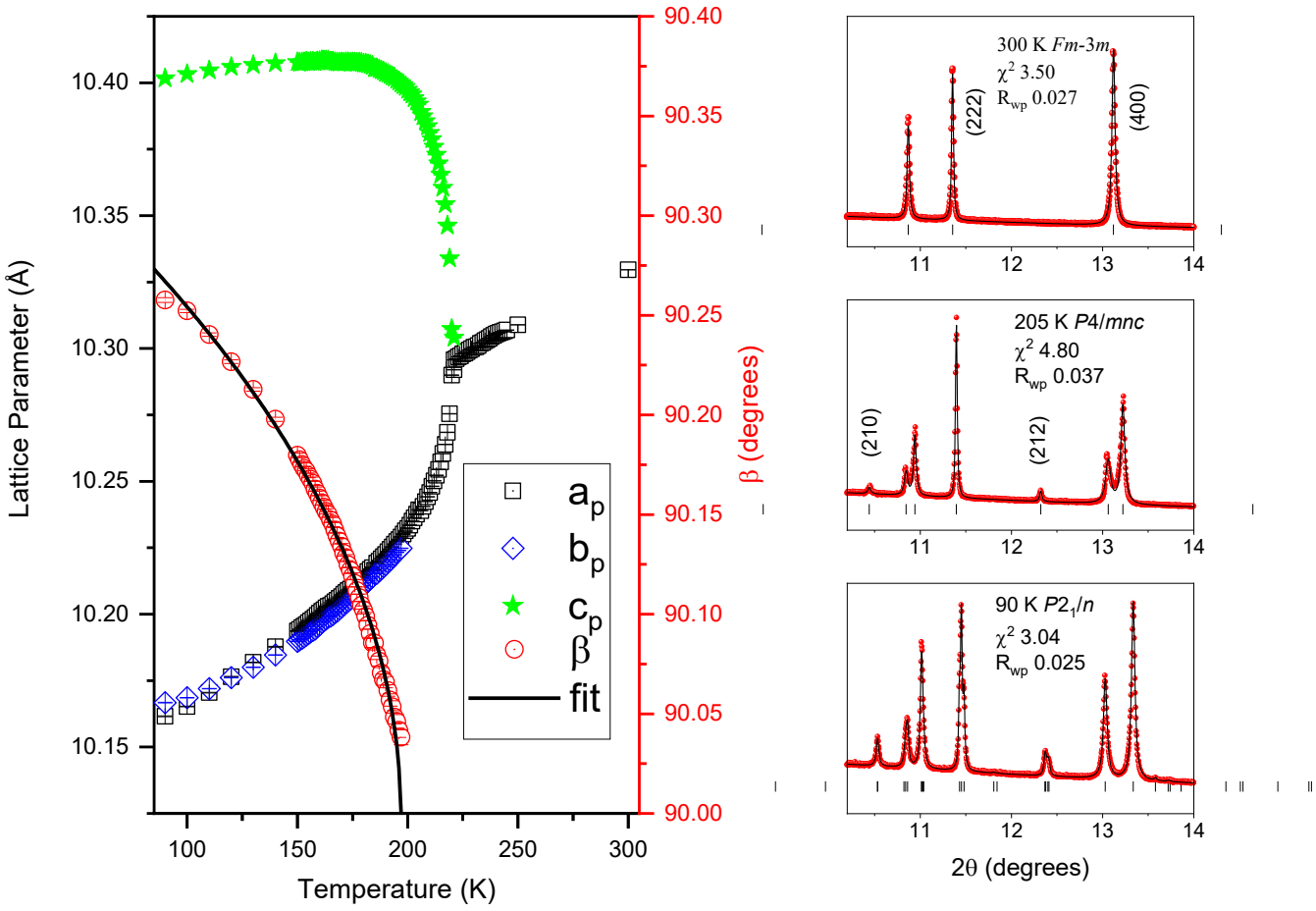

Figure 3. Temperature dependence of the appropriately scaled ($a_p = \sqrt{2}$a, $b_p = \sqrt{2}$b, $c_p = c$), lattice parameters and monoclinic angle for K_2OsBr_6. The data were collected during cooling of the sample from 300 K. The temperature dependence of the beta angle suggests the transition to a tetragonal structure occurs near 197 K. Where not apparent the esds are smaller than the symbols.

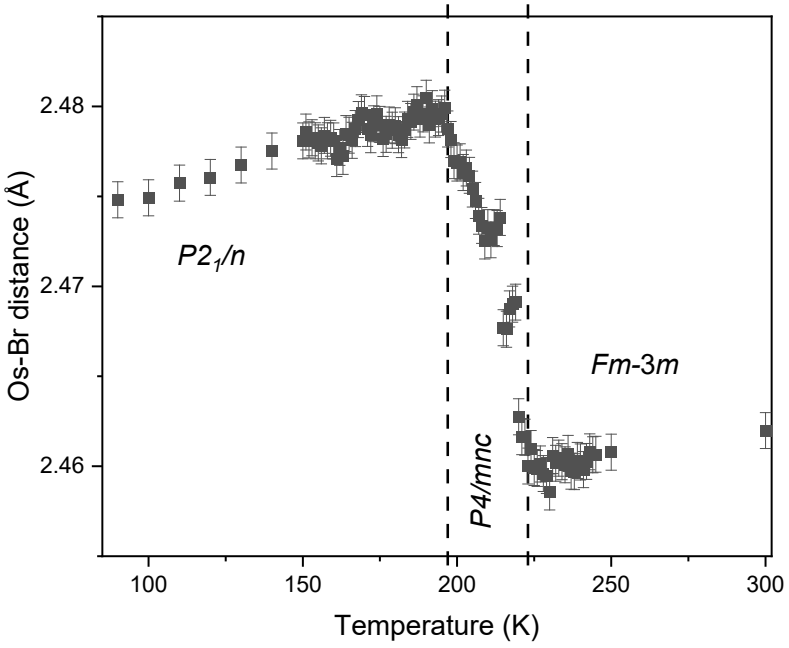

Figure 4. Temperature dependence of the average Os-Br bond distances in K_2OsBr_6 as obtained from Rietveld refinements against S-XRD data. The space groups employed in the Rietveld refinements are indicated.

The structures of all three phases observed in K_2OsBr_6 contain isolated $OsBr_6$ octahedra, that are relatively undistorted. Even in the monoclinic structure the three crystallographically distinct osmium-bromine distances are all very similar, falling in the range 2.457(2) to 2.487(2) Å. The environment of the potassium cation, however, changes dramatically across the three structures. In the cubic structure the potassium is at the centre of a regular KBr_{12} polyhedron with the observed K-Br distance of 3.65405(2) Å at 300 K being similar to the sum of the ionic radii (1.96 and 1.64 Å for 6-coordinate Br and 12-coordinate K respectively). The introduction of the in-phase tilt in the tetragonal structure decreases the effective coordination of the potassium to 8-coordinate with two distinct K-Br distances of 3.4838(9) and 3.61931(5) Å at 200 K, there are a further four long contacts at 3.8197(10) Å. The addition of the out-of-phase tilts in the monoclinic structure further distorts the potassium coordination environment and it can be described as a very distorted KBr_6 polyhedron with an

average K-Br distance of 3.43 Å although there are four longer K-Br contacts between 3.605(5) and 3.781(7) Å at 90 K.

The third example of a vacancy ordered double perovskite studied here is Na_2OsBr_6. This was generated *in-situ* by dehydration of $Na_2OsBr_6.6H_2O$, see below. The diffraction pattern of Na_2OsBr_6 measured at 480 K was indexed to a primitive monoclinic cell with a = 6.97887(3), b = 7.26733(3), c = 10.05055(4) Å, β = 90.665(2) º, Vol = 509.707(5) $Å^3$ corresponding to the monoclinic ($P2_1/n$) structure. This was confirmed by Rietveld analysis, with details of the structure at 90 K given in Table S3. The monoclinic structure was observed to be stable between 80 and 480 K (the limit of our structural investigation). Based on the temperature dependence of the monoclinic angle, Figure 5, a transition to a high symmetry structure is not expected below around 1000 K which is above the sample decomposition temperature. The temperature dependence of the average Os-Br distance is also unusual, Figure 5b. Between 80 and 400 K this distance increases in an approximately linear manner. Above 400 K the average Os-Br distance becomes approximately invariant with temperature. By analogy with K_2OsCl_6 we proposed that this is due to increased rotational disorder. This is evident from the refined anisotropic ADP, that show inhibited displacement parallel to the Os-Br bond, see Figure S4 that is analogous to that seen in cubic K_2OsCl_6. This phase could be recovered to room temperature, allowing its magnetic properties to be investigated and these are described below. The sodium cation is in a $NaBr_6$ polyhedron with an edge sharing arrangement similar to that described for anhydrous Na_2IrCl_6.[9]

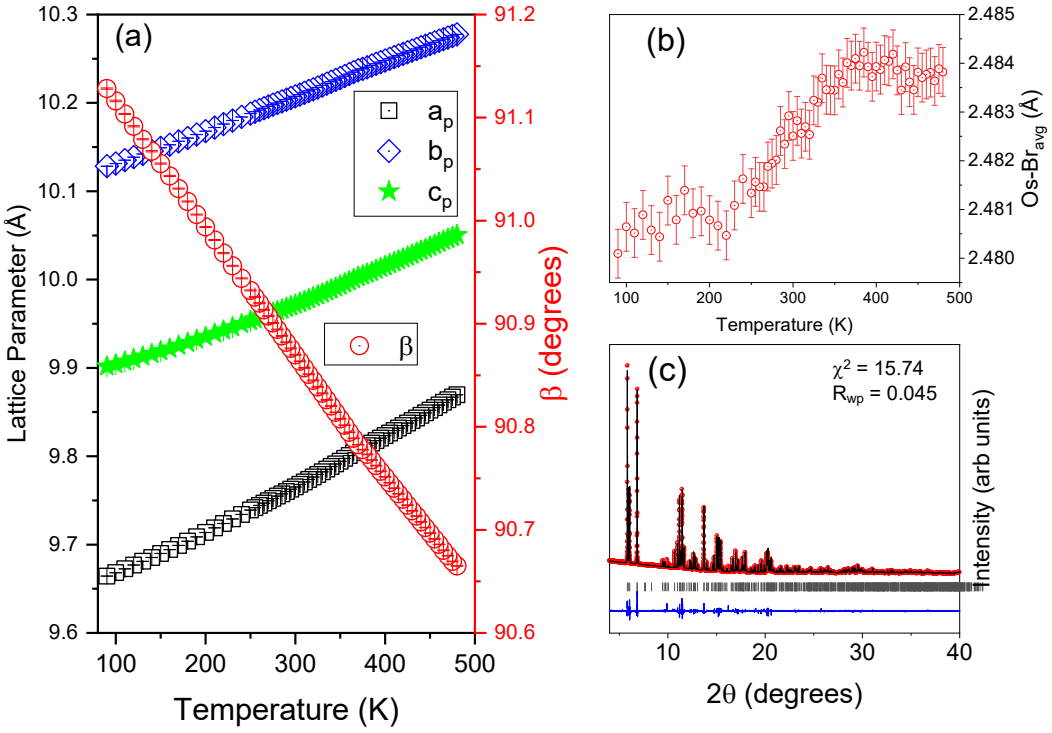

Figure 5. Temperature dependence of (a) the refined unit cell parameters and (b) the average Os-Br distances for Na_2OsBr_6. Panel (c) shows the Rietveld refinement profiles for Na_2OsBr_6 at 90 K. The sample was generated *in-situ* by dehydration of $Na_2OsBr_6.6H_2O$ at 480 K. Where not apparent the esds are smaller than the symbols.

The magnitudes of the symmetry adopted modes were established from the refined structure and these are summarised in Table S2. Remarkably in Na_2OsBr_6 the magnitude of the GM_4^+ mode, that is associated with the out-of-phase tilts is larger than that of the in-phase tilting X_3^+ mode. This is the opposite of that seen in K_2OsBr_6. As demonstrated for some double perovskite type oxides the relative order of these modes $X_3^+ > GM_4^+$ is not impacted by temperature, although the magnitude of the individual modes is, and this serves as a guide to the octahedral tilting patterns that may be present in any intermediate phase.[39] Thus, it can be speculated, but not experimentally verified, that if an intermediate tetragonal phased form between the $P2_1/n$ and $Fm\bar{3}m$ phases in Na_2OsBr_6 it is likely to contain only GM_4^+ out-of-phase tilts. If it was tetragonal, it would be described by space group $I4/m$.

To confirm the feasibility of such a structure we reinvestigated the low temperature structure of K_2OsCl_6 using NPD. These measurements confirm the presence of a symmetry breaking transition near 50 K, see Figure 6, but did not reveal the presence of any reflections indicative of X_3^+ in-phase tilts diagnostic of *P*4/*mnc*. A model in *I*4/*m* with out-of-phase tilts was developed and this gave a satisfactory fit, Figure 6. Structural parameters from the refinement against data measured at 3 K are given in Table S4. Mode analysis shows the GM_4^+ mode to be the strongest mode with the magnitude of 0.260 Å at 3 K. The temperature dependence of this mode was consistent with a second order phase transition.[40]

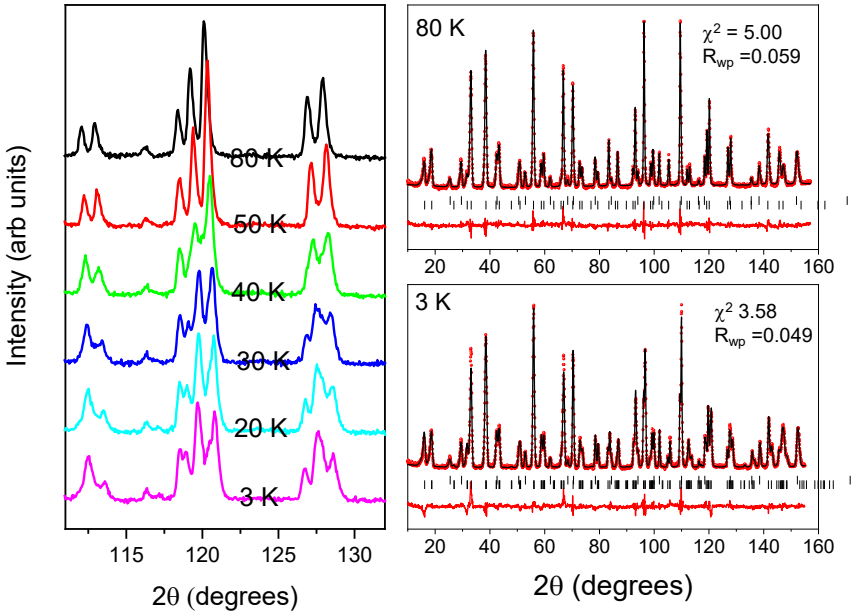

Figure 6. Temperature evolution of selected region of the powder neutron diffraction profiles for K_2OsCl_6 illustrating the change in symmetry below 50 K. The RHS panels illustrate Rietveld profiles. At 80 K the structure was refined in cubic $Fm\bar{3}m$ and at 3 K it was refined in tetragonal *I*4/*m*.

The sense and magnitude of the octahedral rotation in perovskites is dependent on the relative sizes and resulting strains of the cations and anions, the extent of covalent and ionic bonding between the metal cation and the anion and the nature of any intermolecular interactions such as dative coordinate bonding.[41-42] In the simple ABO_3 perovskites the sense

of the tilt is strongly influenced by the formal charges on the two cations. In the 1+:5+ perovskites such as $NaNbO_3$ or $NaTaO_3$ the *M*-point mode condenses first upon cooling the cubic structure resulting in the tetragonal *P*4/*mnc* structure.[43-44] In the 2+:4+ perovskites such as $CaTiO_3$ or $SrRuO_3$ the *I*4/*mcm* structure appears[45-46] as a result of condensation of an R-point mode whereas in 3+:3+ oxides such as $PrAlO_3$ or $NdAlO_3$ the rhombohedral *R*3*c* phase is generally favoured.[47-48] The precise manner by which covalency impacts the octahedral rotation remains unclear. Garcia-Fernandez and co-workers concluded that partial occupancy of the metal t_{2g} orbitals favour rotations.[49] The t_{2g} orbitals have π character with respect to the *M*-*X* bonding involving occupied *np* orbitals of the ligand. Cammaarata and Rondinelli[50] have suggested that increased covalency in the metal-oxygen bond of some ferrates reduces the octahedral rotation and that out-of-phase rotations lead to less covalent character than in-phase rotations

That the symmetry of Na_2OsBr_6 does not change upon heating from 90 to 300 K whereas that of K_2OsBr_6 increases from monoclinic to cubic and K_2OsCl_6 remains cubic over the same temperature range can be understood in terms of the familiar Goldschmidt Tolerance Factor $t = \frac{(r_A+r_X)}{\sqrt{2}(r_B+r_X)}$ where r_A, r_B and r_X are ionic radii for ions in the *A*, *B*, *X* sites. When t = 1.0 the un-tilted cubic structure is expected to be stable. As r_A decreases *t* decreases and tilting of the octahedra becomes favoured. Likewise, as r_X increases *t* decreases.[51] The tolerance factors for the three halides Na_2OsBr_6, K_2OsBr_6 and K_2OsCl_6 are 0.915, 0.982 and 1.000. Based on these, Na_2OsBr_6 is expected to be highly distorted, and K_2OsCl_6 is expected to be cubic. K_2OsBr_6 is intermediate between these two extremes. These expectations are met in the observed phase transition behaviour. Fedorovskiy surveyed the stability of various K_2PtCl_6 type halides and their results show the current osmates fall near the border between the distorted and undistorted structures, although in that work they elected to use the ionic radii values for the six-coordinate *A*-site cation rather than the 12-coordinate values assumed here.[7]

Returning to the temperature dependent behavior of $Na_2OsBr_6{\cdot}6H_2O$, TGA measurements showed the sample lost ~ 4.8 equivalents of water upon heating to 400 K which is less than the six expected. This is similar to the observation for $Na_2IrCl_6.6H_2O$ that lost ~ 3.8 water molecules upon heating to 150 º C (~ 425 K). In the case of $Na_2IrCl_6.6H_2O$ diffraction measurements of the as supplied sample suggest the sample was not single phase;[9] this was not the case for $Na_2OsBr_6{\cdot}6H_2O$. The water molecules were not lost simultaneously from

$Na_2OsBr_6 \cdot 6H_2O$ rather there are three features apparent in the DTGA profile near 327.2, 348.3 and 370.5 K, Figure 7. The thermal evolution of the diffraction patterns between 300 and 480 K, Figure 8, reveal the presence of four distinct regions, namely below 335 K (triclinic), 360-370 K (unidentified) 375-425 K (monoclinic-I) and above 435 K (monoclinic-II). The monoclinic-II phase corresponds to the vacancy ordered double perovskite Na_2OsBr_6 described in space group $P2_1/n$ as above. Regions of phase co-existence between successive pairs of structures were evident. This represents reasonable agreement between the two measurements – noting the different environments, sealed glass capillary for the S-XRD measurements compared to unsealed pan with a flowing dry nitrogen environment for the TGA. The diffraction patterns in three of these four regions were indexed, using the program Conograph, [52] as triclinic or monoclinic as indicated above. The peaks in the second region, 360-370 K, were obviously broader than those in the other three regions and attempts to index these patterns were unsuccessful.

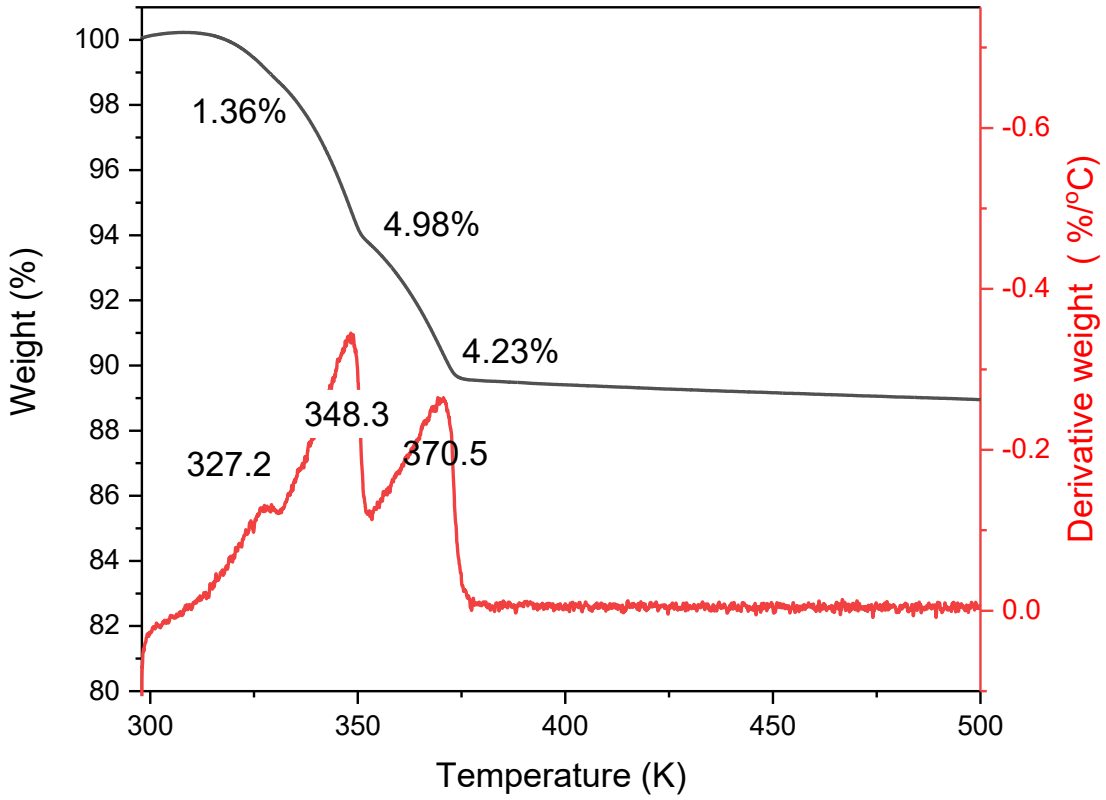

Figure 7. Thermogravimetric curve for $Na_2OsBr_6.6H_2O$. The temperature and weight losses of the transformations are indicated.

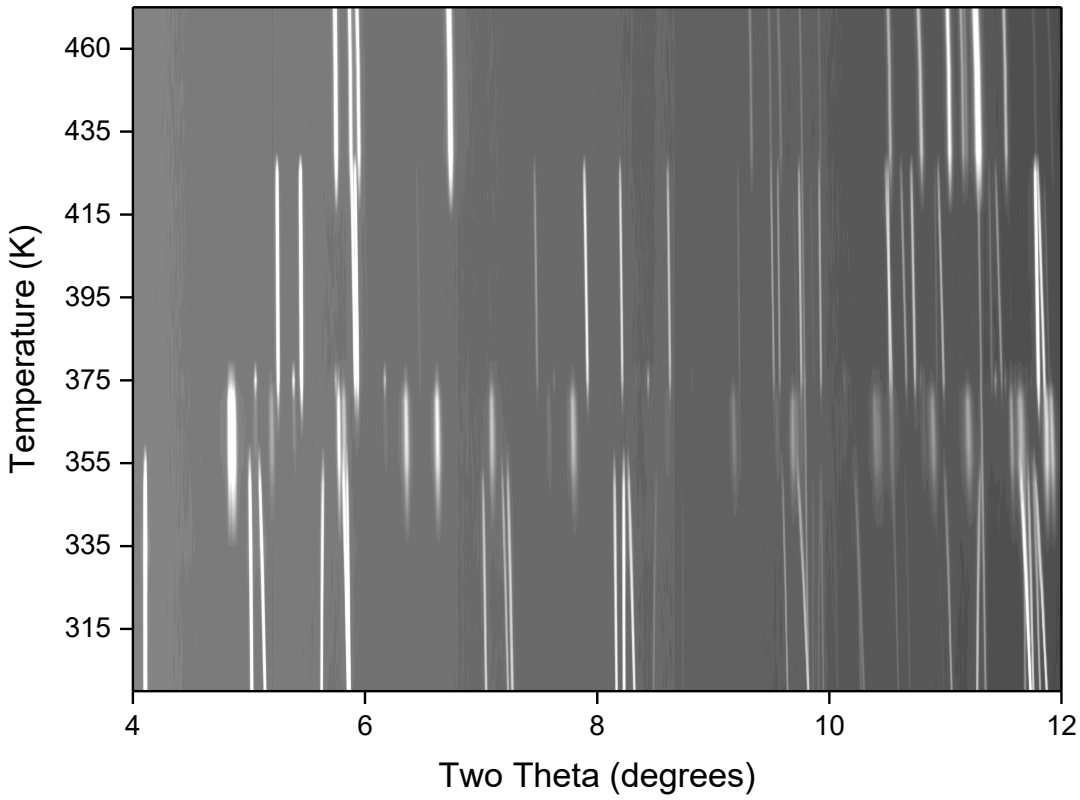

Figure 8. Temperature induced changes in the log of the X-ray scattering intensity for $Na_2OsBr_6.xH_2O$. The sample was ramped from 300 K to 480 K at a rate of 5 K/min. Data were measured for 10 minutes every 5K using X-rays of wavelength 0.590442 Å. Selected profiles are shown in Figure S5.

The S-XRD measurements showed that below 335 K $Na_2OsBr_6 \cdot 6H_2O$ has a triclinic structure $P\bar{1}$ (No. 2), a = 7.051419(20), b = 7.287631(21), c = 8.581013(24) Å, α = 78.49110(20), β = 97.88580(20), γ = 72.56320(20) º Vol = 402.9851(21) $Å^3$ at room temperature. Thus, $Na_2OsBr_6.6H_2O$ is isostructural with several hexachloro complexes including $Na_2IrCl_6.6H_2O$,[9] $Na_2ReCl_6.6H_2O$ [53] and $Na_2PtCl_6.6H_2O$.[54] Rietveld refinement against the synchrotron diffraction data measured at 300 K, taking the reported atomic coordinates for $Na_2ReCl_6.6H_2O$ as a starting model, resulted in a satisfactory fit, as illustrated in Figure S6. Selected structural parameters are given in Table S5, and the structure is shown in Figure 9. Similar quality fits were obtained for the other data sets measured at or below 335

K. Allowing the oxygen occupancies to vary in the Rietveld refinements indicated the water content was 5.9 per Os, that is within the precision of the analysis the sample is best described as a hexa-hydrate.

The triclinic $Na_2OsBr_6 \cdot 6H_2O$ structure contains isolated $OsBr_6$ polyhedra that are separated by Na cations, see Figure 9. The Na cations are in a distorted octahedron consisting of five water molecules and one bromine atom. The Na-O distances are unexceptional and are in the range 2.403(12) – 2.562 (13) Å with the Na-Br distance being considerably longer @ 3.254(8) Å. The $Na(OH_2)_5Br$ polyhedra share edges and the resulting chains are bridged by $[OsBr_6]^{2-}$ anions. The Os-Br distances are in the range 2.4707(19) – 2.5001(19) Å; the average being 2.482 Å. This is similar to the distance observed in K_2OsBr_6.

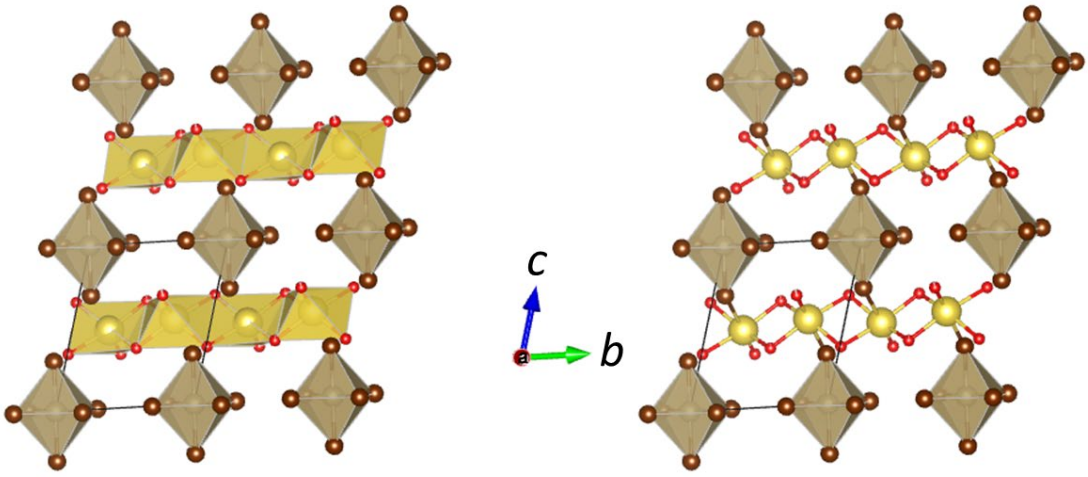

Figure 9. Representation of the structure of $Na_2OsBr_6.6H_2O$ at room temperature. The Os cations are at the centre of the octahedra with the brown spheres representing the Br anions and the red spheres the oxygen atoms. The left hand representation illustrates the displacement of the Na cations in the NaO_5 polyhedra as a result of the formation of a Na-Br bond evident in the right hand representation.

Although it was possible to index the pattern measured at 400 K to a primitive monoclinic cell with a = 6.702054 (17), b = 12.872545 (30), c = 7.461640 (19) Å, β = 108.576(20) º Vol = 610.197(2) $Å^3$ a satisfactory model has not been constructed, see Figure

S7. It proved impossible to recover this phase to room temperature precluding study of its magnetic properties.

2. Magnetic Properties

The temperature dependence of the field cooled (FC) and zero field cooled (ZFC) magnetic susceptibilities for K_2OsCl_6 and K_2OsBr_6 are illustrated in Figure 10. There is little difference between the field cooled and zero field cooled susceptibilities for either compound. The magnetic susceptibility for K_2OsCl_6 is essentially constant above 150 K and only weakly increases below this. This high temperature behaviour is similar to that described by Earnshaw *et al*. and the observed magnetic moment at 300 K (~ 1.4 B.M.) is in reasonable agreement with the value reported by these workers.[55] There is a broad maximum in the susceptibility that occurs near the $I4/m$ to $Fm\bar{3}m$ transition suggesting a weakly magnetic state may be formed at low temperatures. We believe, however, that the correlation between the temperature of the structural transition and the magnetic anomaly is coincidental.

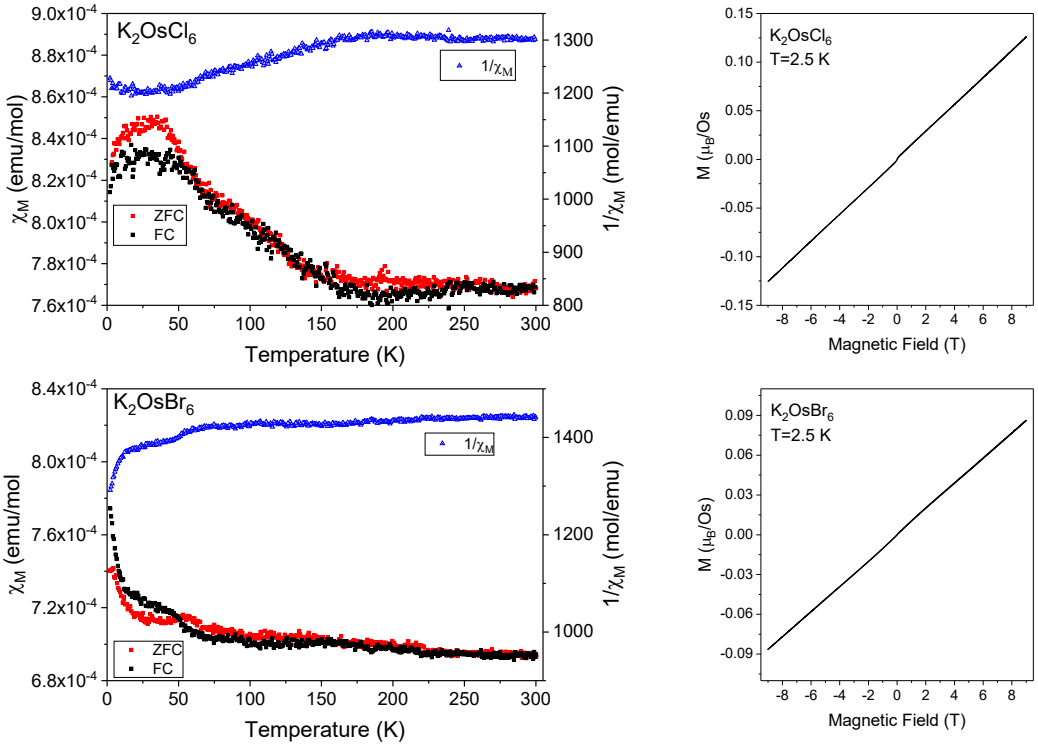

Figure 10. Temperature dependence of the field cooled and zero field cooled magnetic susceptibility for K_2OsCl_6 and K_2OsBr_6 measured with an applied field of 1.0 T. The inverse of the ZFC susceptibility is also shown. The scatter in the data reflects the low measured susceptibilities. The right-hand panels show the field dependence of the magnetisation of the two compounds at 2.5 K.

The magnetic behaviour of K_2OsBr_6 is very similar to that of K_2OsCl_6, with the susceptibilities being essentially independent of temperature above ca 150 K, before increasing slowly at lower temperatures. Whilst a maximum in the susceptibilities is not observed, small anomalies are evident around 50 K that may be indicative of weak magnetic interactions, suggesting that, like K_2OsCl_6, K_2OsBr_6 has a weakly magnetic ground state. The magnetic properties of Na_2OsBr_6 and $Na_2OsBr_6.6H_2O$ are similar and are illustrated in Figure S8. In all cases the inverse susceptibilities clearly do not follow Cure-Weiss type behaviour, see Figure S9-S10.

As evident from Figure 11 the temperature dependence of the magnetic moment is well described by Kotani theory where the effective moment of low-spin d^4 ion in an octahedral environment is given by Equation 1[11],

$$\beta_{eff}^2 = \frac{3\left\{24+\left(\frac{x}{2}-9\right)e^{-\frac{x}{2}}+\left(\frac{5x}{2}-15\right)e^{-\frac{3x}{2}}\right\}}{x\left(1+3e^{-\frac{x}{2}}+5e^{-\frac{3x}{2}}\right)} \quad (1)$$

where $x = \xi/kBT$ and ξ is the spin-orbit coupling strength. This equation has been used to model the magnetic properties of some analogous Ru^{4+} (d^4) halides [13-14, 56] where the spin orbit coupling constant (SOCC) was in the range 1240-1650 cm^{-1}. A similar value was estimated by Lu *et al.* [56] The values estimated for the four Os^{4+} halides studied are considerably higher at around 8500 cm^{-1} (Table 1). The Kotani plots for the four Os^{4+} halides are essentially identical, see Figure 11 and Figure S11. McQueen and co-workers reported a similar occurrence for some isoelectronic ($5d^4$) Ir^V ions. [56]

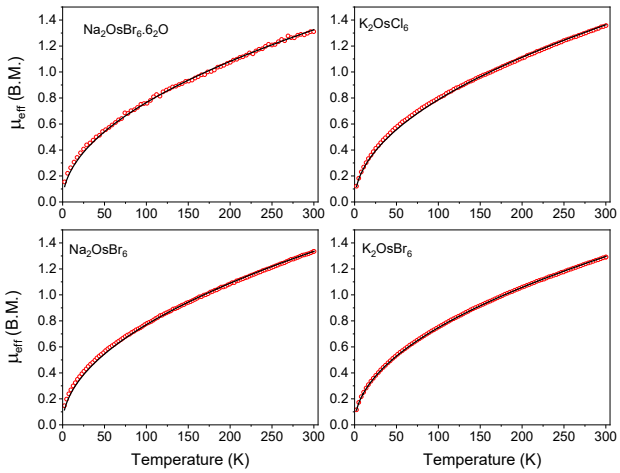

Figure 11. Temperature dependence of the magnetic moments measured under ZFC conditions. The solid black line represents a fit to Kotani theory.

Table 1. Results of fitting the ZFC susceptibilities for A_2OsX_6 halides to Kotani theory

Compound	ξ (cm^{-1})	U_{eff} (BM) @ 300 K
K_2OsCl_6	8077	1.36
K_2OsBr_6	8946	1.29
$Na_2OsBr_6.6H_2O$	8553	1.31
Na_2OsBr_6	8422	1.33

Figgis *et al.* reported similarly high values for the spin-orbit coupling constant for some Os^{4+} halides of the type A_2OsX_6 based on magnetic measurements down to liquid nitrogen temperatures but concluded "that these values are a good deal greater than expected". [15] Subsequently Güdel and co-workers reported a value of ξ = 3000 cm^{-1} for Os^{4+} in Os-doped Cs_2GeF_6 based on spectroscopic analysis.[57] More recently Koseki and co-workers [58] calculated values for ξ for the 5*d* elements using a variety of approaches, finding values of around 7500 cm^{-1} that is only slightly smaller than the values experimentally observed here. These workers highlighted the challenges of calculating SOCC for very heavy 5*d* elements and concluded that low-energy spin-mixed states are likely to be important in influencing the properties.

In the strong SOC limit Os^{4+} has a singlet J_{eff} = 0 ground state and an excited triplet J_{eff} =1 state, the separation between these is dependent on the strength of the spin orbit coupling. Whilst the Kotani model is successful in reproducing the observed temperature dependence of the magnetic moments it masks the more complex low temperature magnetic behaviour shown in Figure 10 which suggests that additional factors apply in the current compounds. Our neutron diffraction measurements show no evidence for any additional features at low temperatures indicative of long-range magnetic ordering, although we note that for 5*d* systems the magnetic form factor is relatively weak. Experimental studies of some isoelectronic iridium (Ir(V) $5d^4$) perovskites have shown some of these have nonmagnetic ground states.[59] The unexpected emergence of such exotic magnetic ground states in Ir^V oxides has been attributed to a number of factors including the effects of non-cubic crystal fields and overlap of the J = 1/2 and J = 3/2 bands (see Scheme 1) leading to partial occupancy of the J = 1/2 state by electrons with an equal number of holes in the J = 3/2 state. The observed tilting of the OsX_6 octahedra will lift the degeneracy of the t_{2g} orbitals, however this splitting is expected to be small compared to both the ligand filed strength and spin orbit coupling, see Figure S1. It seems likely that a J_{eff}

= 0 Γ_1 ground state will occur. Several theoretical studies have predicted a quantum phase transition between the nonmagnetic state and a magnetic state in the double perovskite iridate*s*.[60] Although the present study does not allow us to identify the nature of the magnetic ground state in these osmium halides the observation that the four halides show essentially identical magnetic behaviour despite their vastly different structural distortions indicates that the symmetry lowering plays a relatively minor role in determining the magnetic ground state. Likewise since these compounds are not susceptible to anti-site disorder the impact of such lattice defects can be ignored.[61]

Conclusion

Synchrotron X-ray diffraction methods have been used to establish accurate and precise structures for a family of osmium halides K_2OsCl_6, K_2OsBr_6, Na_2OsBr_6 and $Na_2OsBr_6.6H_2O$. The three anhydrous halides can be described as vacancy-ordered double perovskites. The differences in both their room temperature structures and the presence of thermally induced phase transitions, K_2OsBr_6 undergoes two structural transitions following the sequence $Fm\bar{3}m \rightarrow P4/mnc \rightarrow P2_1/n$, can be understood in terms of the relative size of the constituent ions quantified by the tolerance factor.[7] That K_2OsBr_6 and K_2OsCl_6 display different tetragonal structures with different tilting of the OsX_6 octahedra at low temperatures is unusual and points to the importance of covalent bonding in establishing favoured tilt patterns.

The structure of $Na_2OsBr_6.6H_2O$ has been determined for the first time and the thermal stability of this established using a combination of *in-situ* diffraction and TGA. Although $Na_2OsBr_6.6H_2O$ and Na_2OsBr_6 are isostructural with the analogous iridium chlorides $Na_2IrCl_6.6H_2O$ and Na_2IrCl_6, dehydration proceeds *via* different intermediate phases.[9]

The Os^{4+} cation ($5d^4$) is expected to have a $J_{eff} = 0$ ground state. The magnetic properties of the four compounds display Kotani-like behaviour[11] with large values of the spin-orbit coupling constant. The magnetic susceptibility measurements reveal unusual low temperature properties indicative of a weakly magnetic ground state analogous to that seen in some isoelectronic Ir perovskites.[3] The nature of this magnetic ground state is unknown and it is hoped that this work will stimulate further studies of this unexpected result.

Acknowledgments

We acknowledge the Australian Research Council for support of this work that was facilitated by access to Sydney Analytical, a core research facility at the University of Sydney. This work was, in part, performed at the Powder Diffraction Beamline of the Australian Synchrotron. We thank Dr Rene Macquart for assistance with the magnetic and thermogravimetric analysis. Matilde Saura-Múzquiz gratefully acknowledges the financial support from the Comunidad de Madrid, Spain, through an "Atracción de Talento Investigador" fellowship (2020-T2/IND-20581).

Supporting Information

The Supporting Information is available free of charge at https://pubs.acs.org XXXXXXX

Tables with refined structural parameters for K_2OsCl_6 (90 K and 3 K), Na_2OsBr_6 (90 K) and $Na_2OsBr_6.6H_2O$ (300 K) and summary of mode analysis for K_2OsBr_6 and Na_2OsBr_6. Extended schematic representation of energy splitting for $5d^4$ configuration of the Os^{4+} cation. Examples of Rietveld Fits for S-XRD and NPD data, temperature dependence of R_p and R_{wp} values for K_2OsBr_6 and selected NPD diffraction profiles of $Na_2OsBr_6.6H_2O$ at different temperatures. Representation of the OsX_6 octahedra in K_2OsCl_6 and Na_2OsBr_6 exhibiting refined ADPs. ZFC-FC and field-dependent magnetization curves for $Na_2OsBr_6.6H_2O$ and Na_2OsBr_6, Curie-Weiss fitting of the ZFC curves for K_2OsBr_6 and Na_2OsBr_6, and Kotani plots for the four Os^{4+} $5d^4$ halides K_2OsCl_6, K_2OsBr_6, Na_2OsBr_6 and $Na_2OsBr_6.6H_2O$. (PDF)

References

1. Browne, A. J.; Krajewska, A.; Gibbs, A. S., Quantum materials with strong spin–orbit coupling: challenges and opportunities for materials chemists. *Journal of Materials Chemistry C* **2021,** *9* (35), 11640-11654.

2. Clancy, J. P.; Chen, N.; Kim, C. Y.; Chen, W. F.; Plumb, K. W.; Jeon, B. C.; Noh, T. W.; Kim, Y.-J., Spin-orbit coupling in iridium-based 5*d* compounds probed by x-ray absorption spectroscopy. *Physical Review B* **2012,** *86* (19), 195131.

3. Reig-i-Plessis, D.; Johnson, T. A.; Lu, K.; Chen, Q.; Ruff, J. P. C.; Upton, M. H.; Williams, T. J.; Calder, S.; Zhou, H. D.; Clancy, J. P.; Aczel, A. A.; MacDougall, G. J., Structural, electronic, and magnetic properties of nearly ideal J_{eff} =1/2 iridium halides. *Physical Review Materials* **2020,** *4*, 124407.

4. Guo, S.; Zhong, R.; Wang, W.; Tao, J.; Ni, D.; Cava, R. J., $K_3Ir_2O_6$ and $K_{16.3}Ir_8O_{30}$, Low-Dimensional Iridates with Infinite IrO_6 Chains. *Journal of the American Chemical Society* **2020,** *142* (11), 5389-5395.

5. Ranjbar, B.; Reynolds, E.; Kayser, P.; Kennedy, B. J.; Hester, J. R.; Kimpton, J. A., Structural and Magnetic Properties of the Iridium Double Perovskites $Ba_{2-x}Sr_xYIrO_6$. *Inorganic Chemistry* **2015,** *54* (21), 10468-10476.
6. Ungur, L.; Pallitsch, K.; AlOthman, Z. A.; Al-Kahtani, A. A. S.; Arion, V. B.; Chibotaru, L. F., Towards understanding the magnetism of Os(iv) complexes: an ab initio insight. *Dalton Transactions* **2021,** *50* (36), 12537-12546.
7. Fedorovskiy, A. E.; Drigo, N. A.; Nazeeruddin, M. K., The Role of Goldschmidt's Tolerance Factor in the Formation of A_2BX_6 Double Halide Perovskites and its Optimal Range. *Small Methods* **2020,** *4* (5), 1900426.
8. Khan, N.; Prishchenko, D.; Upton, M. H.; Mazurenko, V. G.; Tsirlin, A. A., Towards cubic symmetry for Ir^{4+}: Structure and magnetism of the antifluorite K_2IrBr_6. *Physical Review B* **2021,** *103* (12), 125158.
9. Bao, S. S.; Wang, D.; Huang, X. D.; Etter, M.; Cai, Z. S.; Wan, X. G.; Dinnebier, R. E.; Zheng, L. M., Na_2IrCl_6 Spin-Orbital-Induced Semiconductor Showing Hydration-Dependent Structural and Magnetic Variations. *Inorganic Chemistry* **2018,** *57* (21), 13252-13258.
10. Johannesen, R. B.; Candela, G. A., Magnetic Susceptibilities and Dilution Effects in Low-Spin d^4 Complexes: Osmium(IV). *Inorganic Chemistry* **1963,** *2* (1), 67-72.
11. Kotani, M., On the magnetic moment of complex ions .1. *Journal of the Physical Society of Japan* **1949,** *4* (4-6), 293-297.
12. Armstrong, R. L.; Mintz, D.; Powell, B. M.; Buyers, W. J. L., Ferrorotative transition in antifluorite crystal K_2OsCl_6. *Physical Review B* **1978,** *17* (3), 1260-1265.
13. Vishnoi, P.; Zuo, J. L.; Cooley, J. A.; Kautzsch, L.; Gomez-Torres, A.; Murillo, J.; Fortier, S.; Wilson, S. D.; Seshadri, R.; Cheetham, A. K., Chemical Control of Spin-Orbit Coupling and Charge Transfer in Vacancy-Ordered Ruthenium(IV) Halide Perovskites. *Angewandte Chemie-International Edition* **2021,** *60* (10), 5184-5188.
14. Vishnoi, P.; Zuo, J. L.; Strom, T. A.; Wu, G.; Wilson, S. D.; Seshadri, R.; Cheetham, A. K., Structural Diversity and Magnetic Properties of Hybrid Ruthenium Halide Perovskites and Related Compounds. *Angewandte Chemie-International Edition* **2020,** *59* (23), 8974-8981.
15. Figgis, B. N.; Lewis, J.; Nyholm, R. S.; Peacock, R. D., The magnetic properties of some d^3, d^4 and d^5 configurations. *Discussions of the Faraday Society* **1958,** *26*, 103-109.
16. Takahashi, H.; Suzuki, H.; Bertinshaw, J.; Bette, S.; Muhle, C.; Nuss, J.; Dinnebier, R.; Yaresko, A.; Khaliullin, G.; Gretarsson, H.; Takayama, T.; Takagi, H.; Keimer, B., Nonmagnetic J=0 State and Spin-Orbit Excitations in K_2RuCl_6. *Physical Review Letters* **2021,** *127* (22), 227201.
17. Stranks, S. D.; Snaith, H. J., Metal-halide perovskites for photovoltaic and light-emitting devices. *Nature Nanotechnology* **2015,** *10* (5), 391-402.
18. McClure, E. T.; Ball, M. R.; Windl, W.; Woodward, P. M., Cs_2AgBiX_6 (X = Br, Cl): New Visible Light Absorbing, Lead-Free Halide Perovskite Semiconductors. *Chemistry of Materials* **2016,** *28* (5), 1348-1354.
19. Majher, J. D.; Gray, M. B.; Liu, T.; Holzapfel, N. P.; Woodward, P. M., Rb_3InCl_6: A Monoclinic Double Perovskite Derivative with Bright Sb^{3+}-Activated Photoluminescence. *Inorganic Chemistry* **2020,** *59* (19), 14478-14485.
20. Maughan, A. E.; Ganose, A. M.; Candia, A. M.; Granger, J. T.; Scanlon, D. O.; Neilson, J. R., Anharmonicity and Octahedral Tilting in Hybrid Vacancy-Ordered Double Perovskites. *Chemistry of Materials* **2018,** *30* (2), 472-483.
21. Kayser, P.; Injac, S.; Kennedy, B. J.; Vogt, T.; Avdeev, M.; Maynard-Casely, H. E.; Zhang, Z., Structural and Magnetic Properties of the Osmium Double Perovskites $Ba_{2-x}Sr_xYOsO_6$. *Inorganic Chemistry* **2017,** *56* (11), 6565-6575.

22. Wallwork, K. S.; Kennedy, B. J.; Wang, D. In *The high resolution powder diffraction beamline for the Australian Synchrotron*, 9th International Conference on Synchrotron Radiation Instrumentation (SRI 2006), Daegu, South Korea, May 28-Jun 02; Daegu, South Korea, 2006; p 879.
23. Thompson, P.; Cox, D. E.; Hastings, J. B., Rietveld refinement of Debye-Scherrer synchrotron X-ray data from Al_2O_3. *Journal of Applied Crystallography* **1987,** *20* (2), 79-83.
24. Avdeev, M.; Hester, J. R., ECHIDNA: a decade of high-resolution neutron powder diffraction at OPAL. *Journal of Applied Crystallography* **2018,** *51*, 1597-1604.
25. Larson, A. C.; Von Dreele, R. B., GSAS. *General Structure Analysis System. LANSCE, MS-H805, Los Alamos, New Mexico* **1994**.
26. Toby, B. H., EXPGUI, a graphical user interface for GSAS. *J. Appl. Cryst.* **2001,** *34*, 210-213.
27. Orobengoa, D.; Capillas, C.; Aroyo, M. I.; Perez-Mato, J. M., AMPLIMODES: symmetry-mode analysis on the Bilbao Crystallographic Server. *Journal of Applied Crystallography* **2009,** *42*, 820-833.
28. Khan, N.; Prishchenko, D.; Skourski, Y.; Mazurenko, V. G.; Tsirlin, A. A., Cubic symmetry and magnetic frustration on the fcc spin lattice in K_2IrCl_6. *Physical Review B* **2019,** *99* (14), 144425.
29. Bolzan, A. A.; Fong, C.; Kennedy, B. J.; Howard, C. J., Structural studies of rutile-type metal dioxides. *Acta Crystallographica Section B-Structural Science* **1997,** *53*, 373-380.
30. Chay, C.; Avdeev, M.; Brand, H. E. A.; Injac, S.; Whittle, T. A.; Kennedy, B. J., Crystal structures and phase transition behaviour in the 5d transition metal oxides $AReO_4$ (A = Ag, Na, K, Rb, Cs and Tl). *Dalton Transactions* **2019,** *48* (47), 17524-17532.
31. Kennedy, B. J.; Injac, S.; Thorogood, G. J.; Brand, H. E. A.; Poineau, F., Structures and Phase Transitions in Pertechnetates. *Inorganic Chemistry* **2019,** *58* (15), 10119-10128.
32. Rabuffetti, F. A.; Culver, S. P.; Suescun, L.; Brutchey, R. L., Structural Disorder in $AMoO_4$ (A = Ca, Sr, Ba) Scheelite Nanocrystals. *Inorganic Chemistry* **2014,** *53* (2), 1056-1061.
33. Greve, B. K.; Martin, K. L.; Lee, P. L.; Chupas, P. J.; Chapman, K. W.; Wilkinson, A. P., Pronounced Negative Thermal Expansion from a Simple Structure: Cubic ScF_3. *Journal of the American Chemical Society* **2010,** *132* (44), 15496-15498.
34. Turner, A. G.; Clifford, A. F.; Rao, C. N. R., Potassium hexachloro-osmate, K_2OsCl_6, and potassium hexabromo-osmate, K_2OsBr_6. *Analytical Chemistry* **1958,** *30* (10), 1708-1709.
35. Glazer, A. M., Classification of tilted octahedra in perovskites. *Acta Crystallographica Section B-Structural Science* **1972,** *B 28*, 3384-3392.
36. Boysen, H.; Hewat, A. W., Neutron powder investigation of structural-changes in K_2SnCl_6. *Acta Crystallographica Section B-Structural Science* **1978,** *34*, 1412-1418.
37. Howard, C. J.; Kennedy, B. J.; Woodward, P. M., Ordered double perovskites - a group-theoretical analysis. *Acta Crystallographica Section B-Structural Science* **2003,** *59*, 463-471.
38. Arulnesan, S. W.; Kayser, P.; Kimpton, J. A.; Kennedy, B. J., Studies of the fergusonite to scheelite phase transition in $LnNbO_4$ orthoniobates. *Journal of Solid State Chemistry* **2019,** *277*, 229-239.
39. Zhou, Q. D.; Kennedy, B. J.; Avdeev, M., Crystal structures and phase transitions in Sr_2InTaO_6 perovskite. *Physics and Chemistry of Minerals* **2013,** *40* (8), 603-610.
40. Sutton, M.; Armstrong, R. L.; Powell, B. M.; Buyers, W. J. L., Lattice-dynamics and phase-transitions in antifluorite crystals - K_2OsCl_6. *Physical Review B* **1983,** *27* (1), 380-390.
41. Varadwaj, P. R.; Varadwaj, A.; Marques, H. M.; Yamashita, K., Significance of hydrogen bonding and other noncovalent interactions in determining octahedral tilting in the CH3NH3PbI3 hybrid organic-inorganic halide perovskite solar cell semiconductor. *Scientific Reports* **2019,** *9* (1), 50.
42. Woodward, P., Octahedral Tilting in Perovskites. II. Structure Stabilizing Forces. *Acta Crystallographica Section B* **1997,** *53* (1), 44-66.

43. Kennedy, B. J.; Prodjosantoso, A. K.; Howard, C. J., Powder neutron diffraction study of the high temperature phase transitions in $NaTaO_3$. *Journal of Physics-Condensed Matter* **1999,** *11* (33), 6319-6327.
44. Darlington, C. N. W.; Knight, K. S., High-temperature phases of $NaNbO_3$ and $NaTaO_3$. *Acta Crystallographica Section B-Structural Science* **1999,** *55*, 24-30.
45. Kennedy, B. J.; Howard, C. J.; Chakoumakos, B. C., Phase transitions in perovskite at elevated temperatures - a powder neutron diffraction study. *Journal of Physics-Condensed Matter* **1999,** *11* (6), 1479-1488.
46. Kennedy, B. J.; Hunter, B. A.; Hester, J. R., Synchrotron x-ray diffraction reexamination of the sequence of high-temperature phases in $SrRuO_3$. *Physical Review B* **2002,** *65* (22), 224103.
47. Carpenter, M. A.; Howard, C. J.; Kennedy, B. J.; Knight, K. S., Strain mechanism for order-parameter coupling through successive phase transitions in $PrAlO_3$. *Physical Review B* **2005,** *72* (2), 024118.
48. Howard, C. J.; Kennedy, B. J.; Chakoumakos, B. C., Neutron powder diffraction study of rhombohedral rare-earth aluminates and the rhombohedral to cubic phase transition. *Journal of Physics-Condensed Matter* **2000,** *12* (4), 349-365.
49. Garcia-Fernandez, P.; Aramburu, J. A.; Barriuso, M. T.; Moreno, M., Key Role of Covalent Bonding in Octahedral Tilting in Perovskites. *The Journal of Physical Chemistry Letters* **2010,** *1* (3), 647-651.
50. Cammarata, A.; Rondinelli, J. M., Covalent dependence of octahedral rotations in orthorhombic perovskite oxides. **2014,** *141* (11), 114704.
51. Maughan, A. E.; Ganose, A. M.; Almaker, M. A.; Scanlon, D. O.; Neilson, J. R., Tolerance Factor and Cooperative Tilting Effects in Vacancy-Ordered Double Perovskite Halides. *Chemistry of Materials* **2018,** *30* (11), 3909-3919.
52. Oishi-Tomiyasu, R., Robust powder auto-indexing using many peaks. *Journal of Applied Crystallography* **2014,** *47*, 593-598.
53. Shusharina, E. A.; Zadesenets, A. V.; Gromilov, S. A., Crystal structure and thermal properties of $Na_2[ReCl_6]\cdot 6H_2O$. *Journal of Structural Chemistry* **2011,** *52* (2), 439-442.
54. Miyoshi, H.; Horiuchi, K.; Sakagami, N.; Okamoto, K.; Ikeda, R., 35Cl NQR, 1H NMR, and X-Ray Diffraction Studies in a Hydrogen Bonded Complex $Na_2PtCl_6 \cdot 6H_2O$ %. *Zeitschrift für Naturforschung A* **1998,** *53* (6-7), 603-607.
55. Earnshaw, A.; Figgis, B. N.; Lewis, J.; Peacock, R. D., 601. The magnetic properties of some d^4-complexes. *Journal of the Chemical Society* **1961**, 3132-3138.
56. Lu, H.; Chamorro, J. R.; Wan, C.; McQueen, T. M., Universal Single-Ion Physics in Spin–Orbit-Coupled d^5 and d^4 Ions. *Inorganic Chemistry* **2018,** *57* (22), 14443-14449.
57. Wermuth, M.; Reber, C.; Güdel, H. U., High-Resolution Luminescence and Absorption Spectroscopy of Cs_2GeF_6:$Os4^+$. *Inorganic Chemistry* **2001,** *40* (15), 3693-3703.
58. Koseki, S.; Matsunaga, N.; Asada, T.; Schmidt, M. W.; Gordon, M. S., Spin–Orbit Coupling Constants in Atoms and Ions of Transition Elements: Comparison of Effective Core Potentials, Model Core Potentials, and All-Electron Methods. *The Journal of Physical Chemistry A* **2019,** *123* (12), 2325-2339.
59. Terzic, J.; Zheng, H.; Ye, F.; Zhao, H. D.; Schlottmann, P.; De Long, L. E.; Yuan, S. J.; Cao, G., Evidence for a low-temperature magnetic ground state in double-perovskite iridates with $Ir^{5+}(5d^4)$ ions. *Physical Review B* **2017,** *96* (6), 064436.
60. Bhaskaran, L.; Ponomaryov, A. N.; Wosnitza, J.; Khan, N.; Tsirlin, A. A.; Zhitomirsky, M. E.; Zvyagin, S. A., Antiferromagnetic resonance in the cubic iridium hexahalides $(NH_4)_2IrCl_6$ and K_2IrCl_6. *Physical Review B* **2021,** *104* (17), 184404.

61. Chen, Q.; Svoboda, C.; Zheng, Q.; Sales, B. C.; Mandrus, D. G.; Zhou, H. D.; Zhou, J. S.; McComb, D.; Randeria, M.; Trivedi, N.; Yan, J. Q., Magnetism out of antisite disorder in the J = 0 compound Ba_2YIrO_6. *Physical Review B* **2017,** *96* (14), 144423.

For Table of Content Only

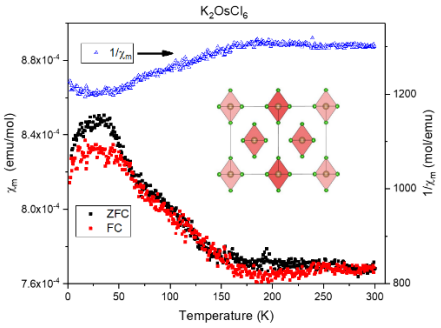

The structures and magnetic properties of some Os^{4+} ($5d^4$) vacancy-ordered double perovskites halides, K_2OsCl_6, K_2OsBr_6, Na_2OsBr_6 and $Na_2OsBr_6.6H_2O$ are described. These display a variety of temperature induced structural phase transitions. They display Kotani-like behaviour, consistent with a $J_{eff} = 0$ ground state, although their low temperature properties suggest a weakly magnetic ground state.